Supplementary Material

$Cr_3X_2Y_2$ (X, Y = S, Se, Te) Monolayers: Valley-Polarized Quantum Anomalous Hall Insulator Driven by Electric Field

Xiaojing Yao,[1] Yinong Liu,[1] Huijie Lian,[1] Jinlian Lu,[3] Xiaokang Xu,[2,4*] Ailei He,[2*] Xiuyun Zhang[2*]

[1]College of Physics and Hebei Advanced Thin Films Laboratory, Hebei Normal University, Shijiazhuang 050024, China.

[2]College of Physics Science and Technology, Yangzhou University, Yangzhou 225002, China.
[3]Department of Physics, Yancheng Institute of Technology, Yancheng 224051, China.
[4]Key Laboratory of Quantum Materials and Devices of Ministry of Education, School of Physics, Southeast University, Nanjing 211189, China.

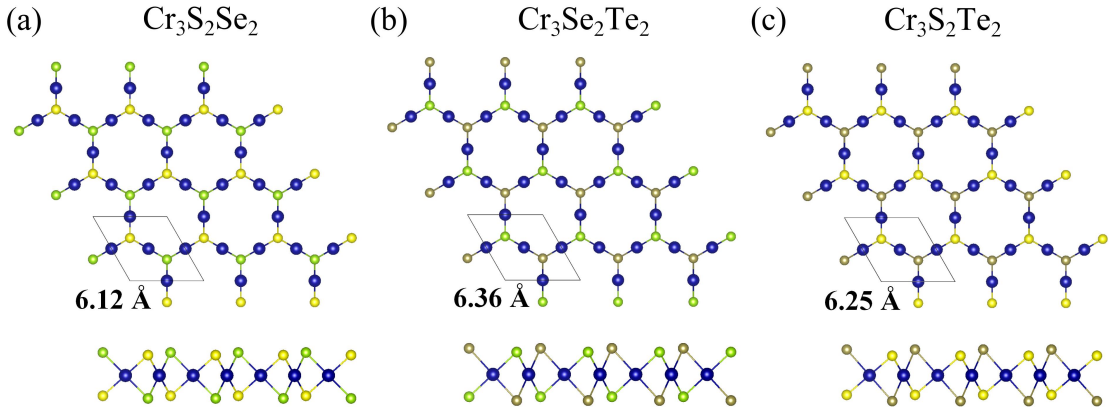

Figure S1. Top and side views of $Cr_3S_2Se_2$ (a), $Cr_3Se_2Te_2$ (b) and $Cr_3S_2Te_2$ (c) monolayers, respectively.

Table S1. The lattice constant (L, Å), Cr-X/Y bond lengths (d_1, d_2, Å) and the Cr-X/Y-Cr bond angles (θ_1, θ_2, degree) of $Cr_3X_2Y_2$ monolayers as shown in Figure 1a.

sys	L	d_1	d_2	θ_1	θ_2
$Cr_3S_2Se_2$	6.12	2.37	2.51	75.0	80.2
$Cr_3Se_2Te_2$	6.36	2.52	2.72	71.5	78.5
$Cr_3S_2Te_2$	6.25	2.37	2.72	70.0	82.2

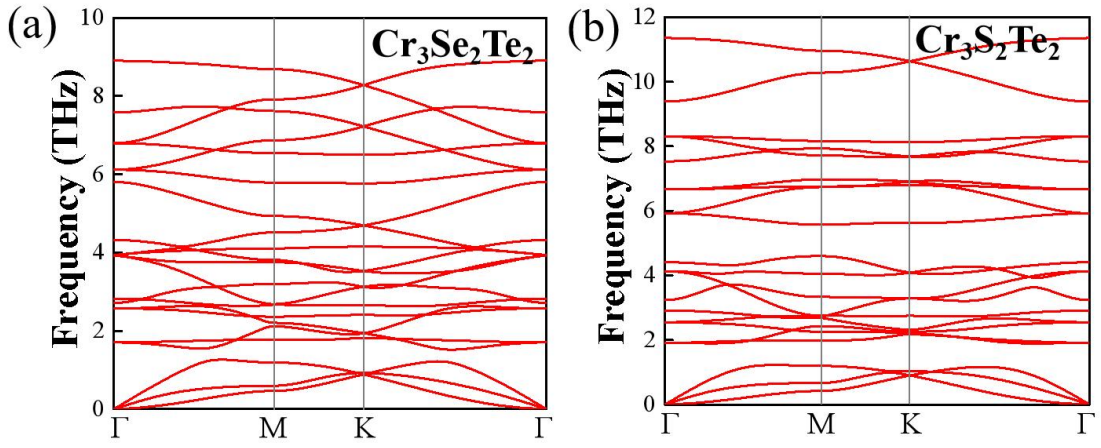

Figure S2. The phonon spectra for $Cr_3Se_2Te_2$ (a) and $Cr_3S_2Te_2$ (b) monolayers.

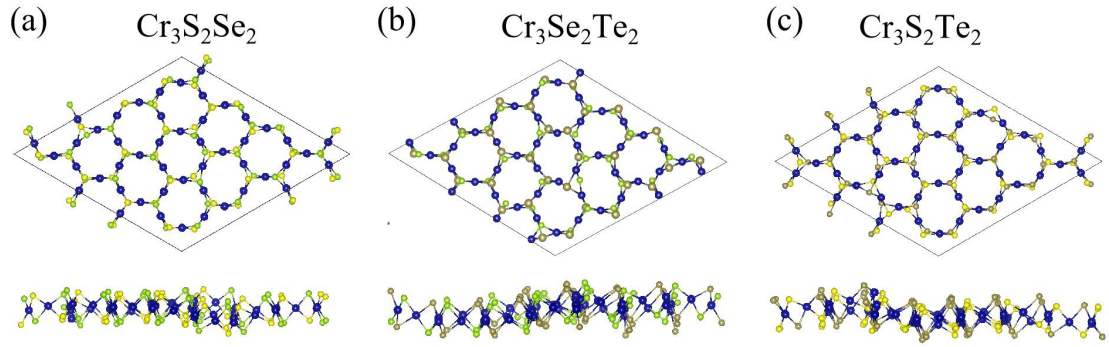

Figure S3. The structures of $Cr_3S_2Se_2$ (a), $Cr_3Se_2Te_2$ (b) and $Cr_3S_2Te_2$ (c) at end of 6 *ps* at 300 K during AIMD simulation.

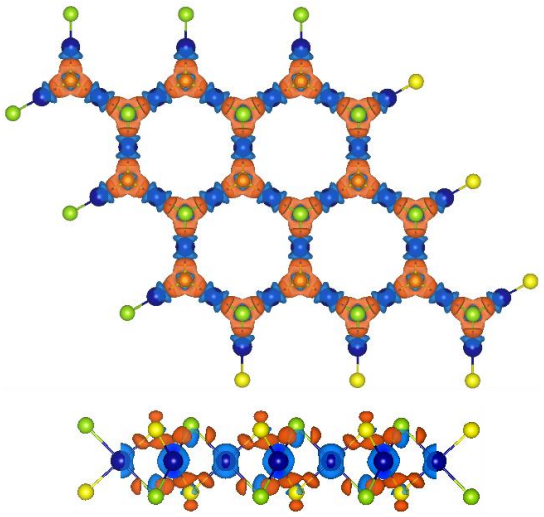

Figure S4. Charge density of difference of $Cr_3S_2Se_2$ monolayer, the orange and blue colors represent electron accumulation and depletion, respectively.

Table S2. The elastic constants C_{11}, C_{12}, C_{22} and C_{66}. *J* is the nearest neighboring exchange coupling parameter (unit, eV).

sys	C_{11}	C_{12}	C_{22}	C_{66}	*J*
$Cr_3S_2Se_2$	26.97	18.84	26.97	4.06	0.011
$Cr_3Se_2Te_2$	18.93	16.89	18.93	1.02	0.009
$Cr_3S_2Te_2$	21.36	17.95	21.36	1.71	0.011

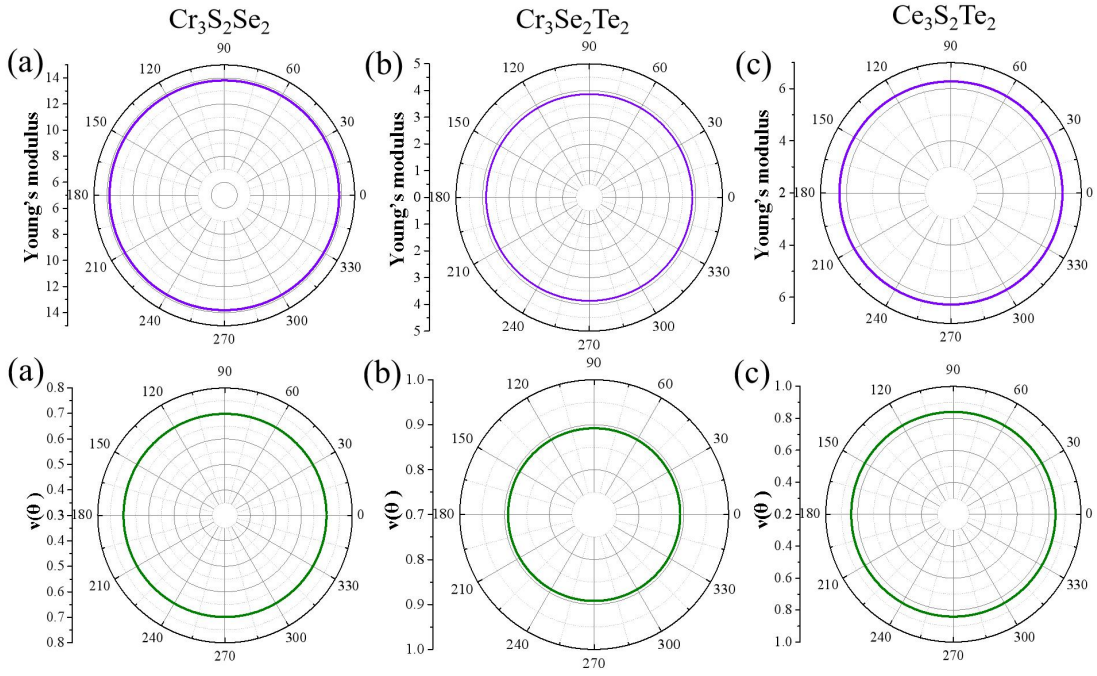

Figure S5. Young's modulus and Poisson's ratio of $Cr_3X_2Y_2$ monolayers as a function of the angle θ. θ=0° corresponds to the *x*-axis.

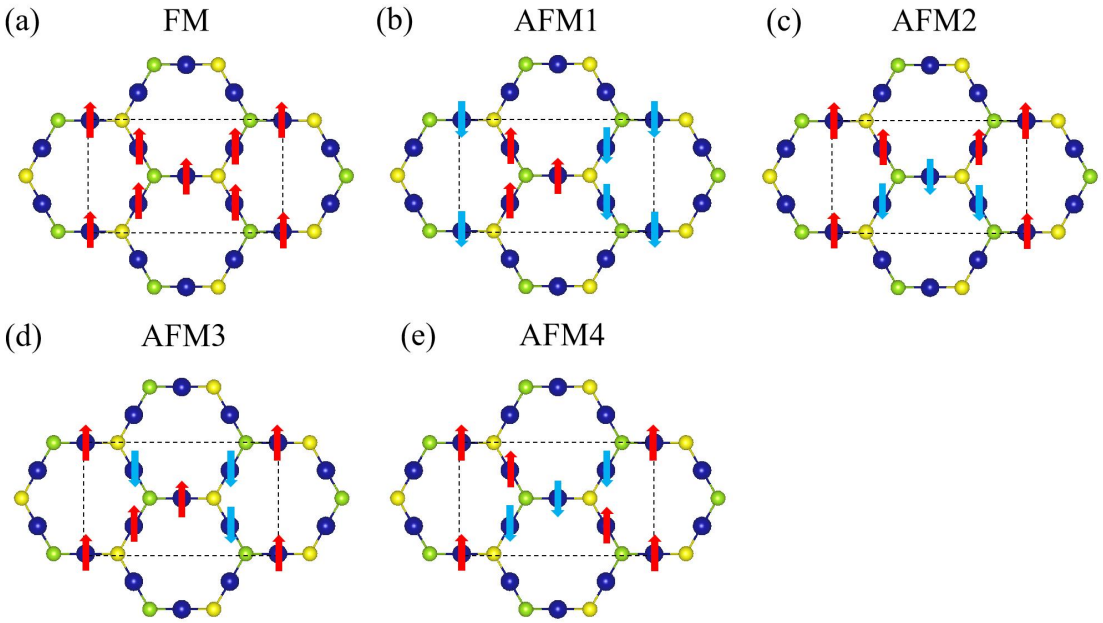

Figure S6. Considered ferromagnetic and four antiferromagnetic configurations for $Cr_3X_2Y_2$ (X, Y = S, Se, Te) monolayers.

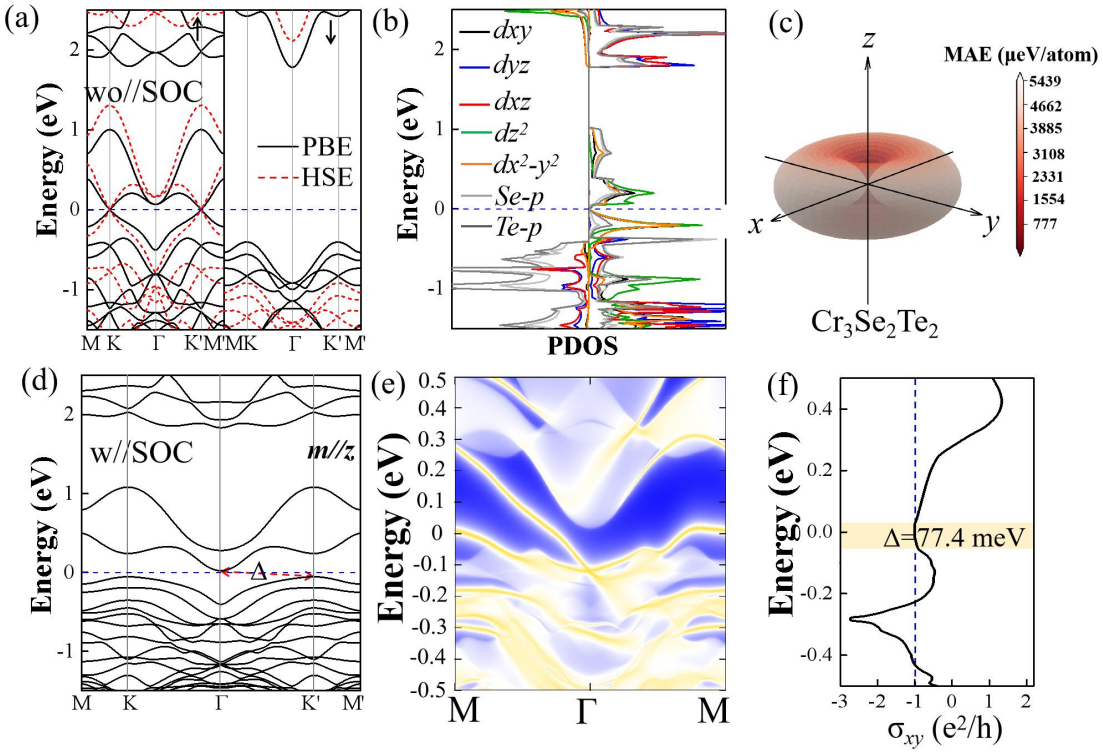

Figure S7. Band structure of $Cr_3Se_2Te_2$ monolayers without (a) and with (d) considering SOC effect (m//*z*). Projected density of state (b), MAE (c), edge states (e) and anomalous Hall conductivity (AHC) (f) of $Cr_3Se_2Te_2$ monolayer.

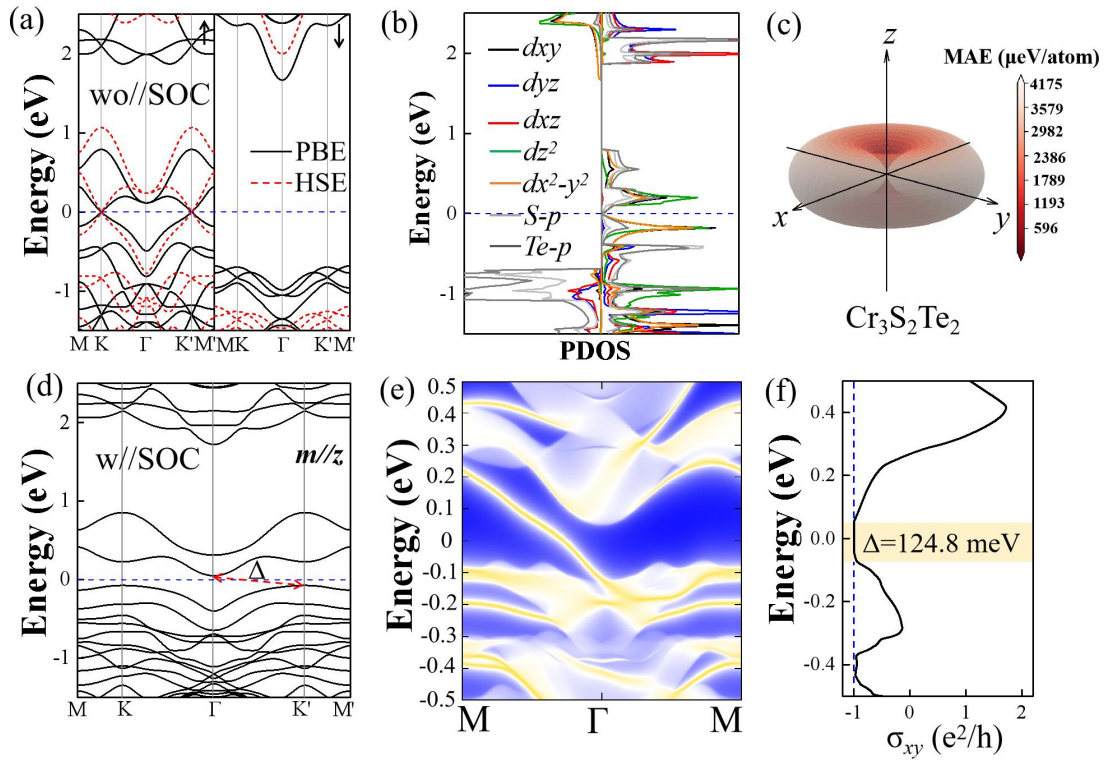

Figure S8. Band structure of $Cr_3S_2Te_2$ monolayers without (a) and with (d) considering SOC effect (*m*//*z*). Projected density of state (b), MAE (c), edge states (e) and anomalous Hall conductivity (AHC) (f) of $Cr_3S_2Te_2$ monolayer.

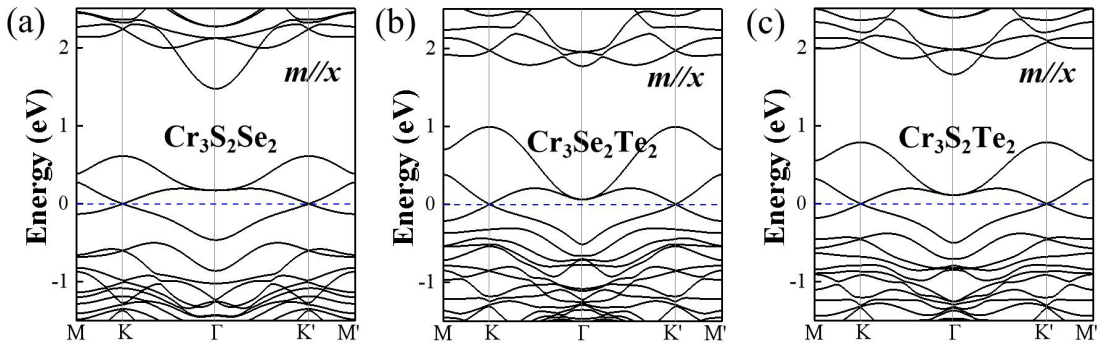

Figure S9. Band structure of $Cr_3X_2Y_2$ monolayers with considering SOC effect (*m*//*x*).

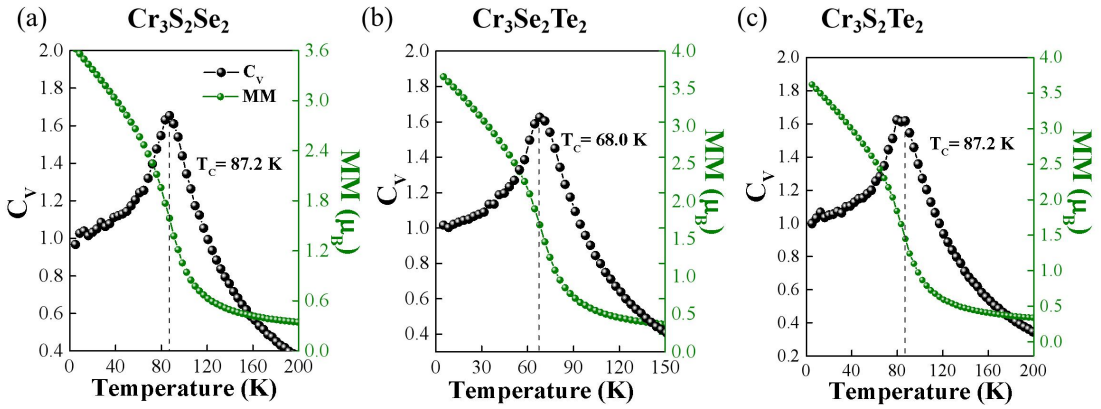

Figure S10. The specific heat (C_V) and magnetic moment as as function of temperature for $Cr_3S_2Se_2$ (a), $Cr_3Se_2Te_2$ (b) and $Cr_3S_2Te_2$ (c) monolayers.

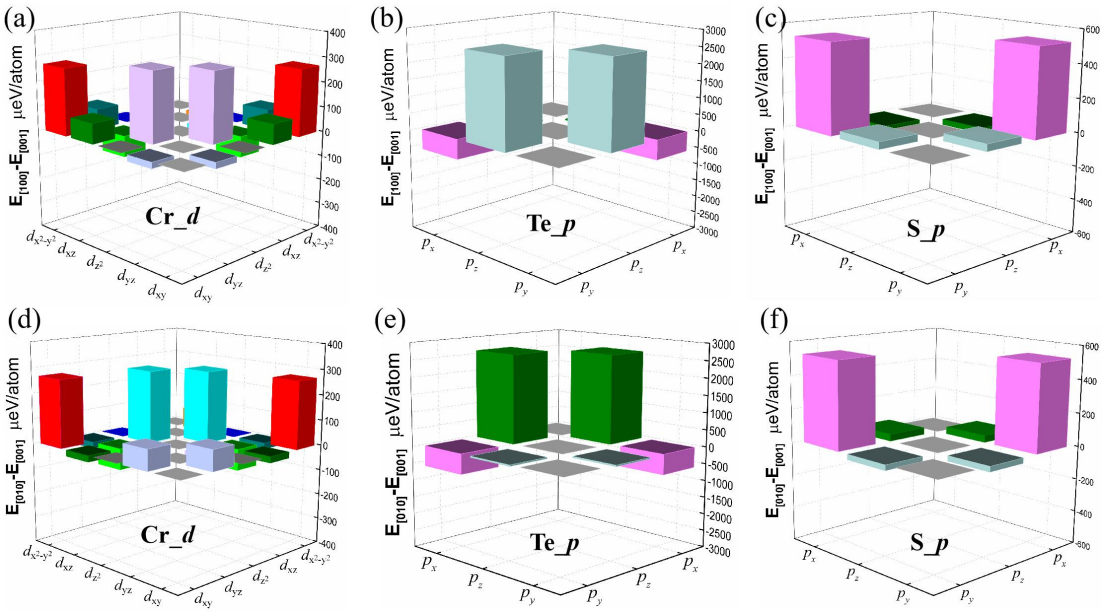

Figure S11. The contribution to MAE from the SOC interaction between Cr-*d*, Se-*p* and Te-*p* orbitals along [100] (a) and [010] (b) directions for $Cr_3Se_2Te_2$ monolayer. The energy is referenced to the [001] direction.

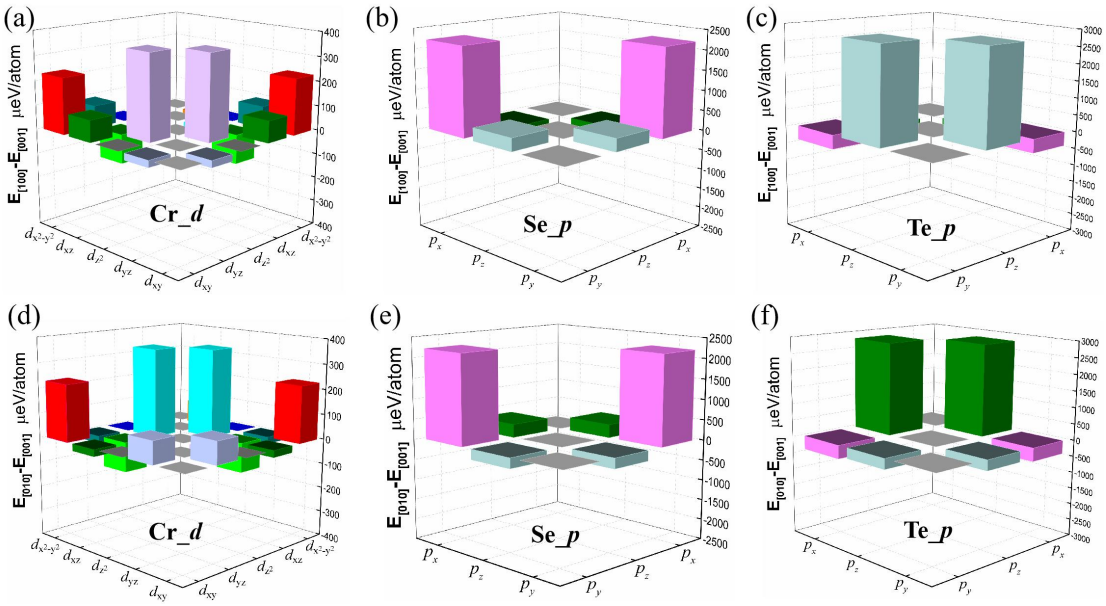

Figure S12. The contribution to MAE from the SOC interaction between Cr-*d*, Se-*p* and Te-*p* orbitals along [100] (a) and [010] (b) directions for $Cr_3S_2Te_2$ monolayer. The energy is referenced to the [001] direction.

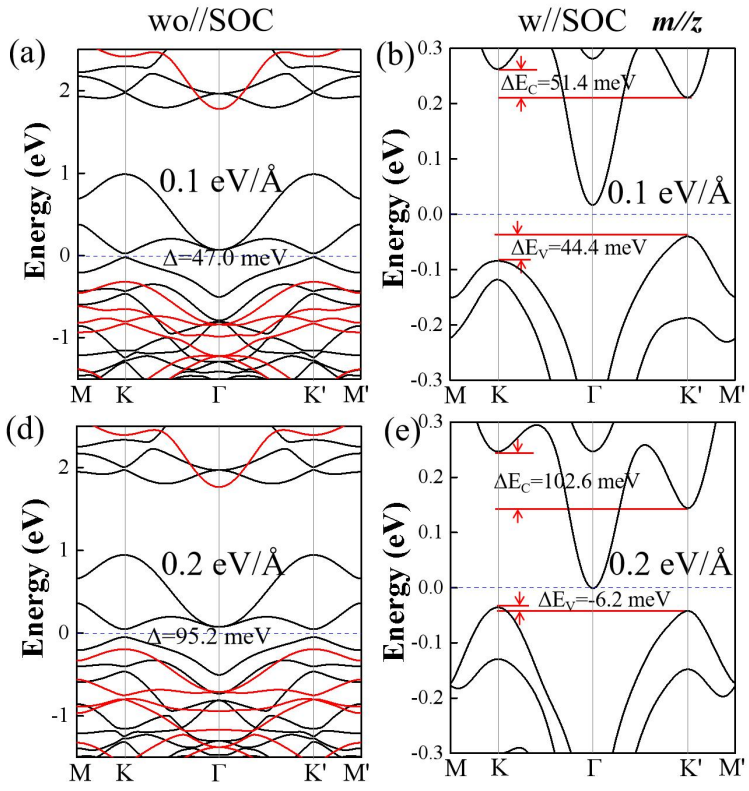

Figure S13. Band structures of $Cr_3Se_2Te_2$ monolayer without (a,d) and with (b,e) considering SOC effect under electric field of 0.1 eV/Å and 0.2 eV/Å.

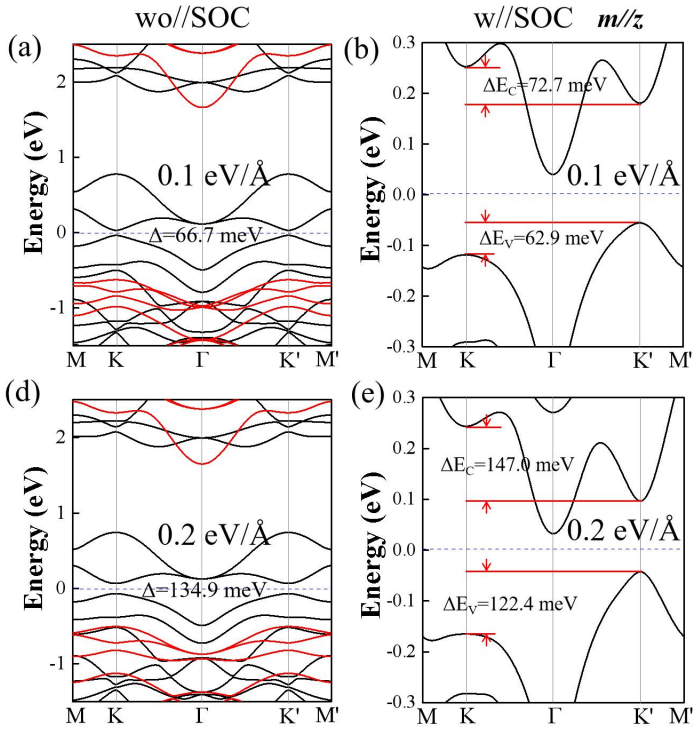

Figure S14. Band structures of $Cr_3S_2Te_2$ monolayer without (a,d) and with (b,e) considering SOC effect under electric field of 0.1 eV/Å and 0.2 eV/Å.

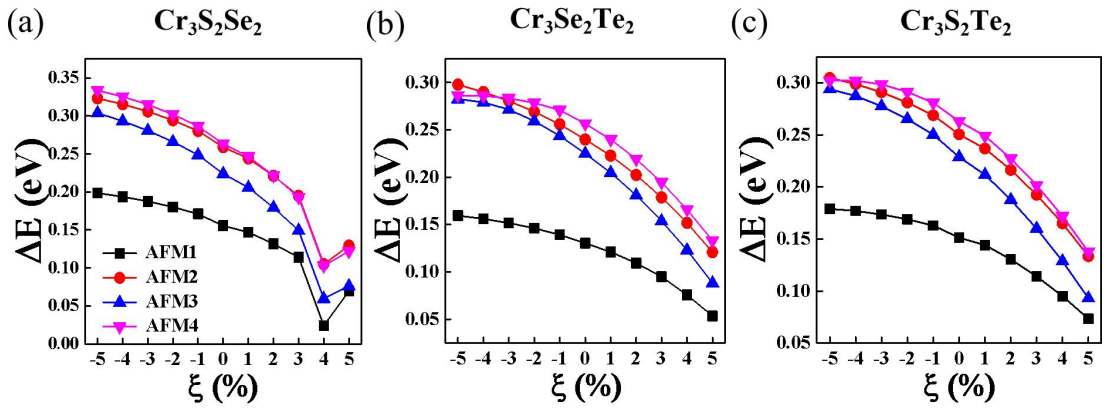

Figure S15. The energy differences ($\Delta E=E_{AFM}-E_{FM}$, eV/f. u.) between FM and AFM states of $Cr_3X_2Y_2$ monolayers under biaxial strains. The energy of FM state is 0 eV.

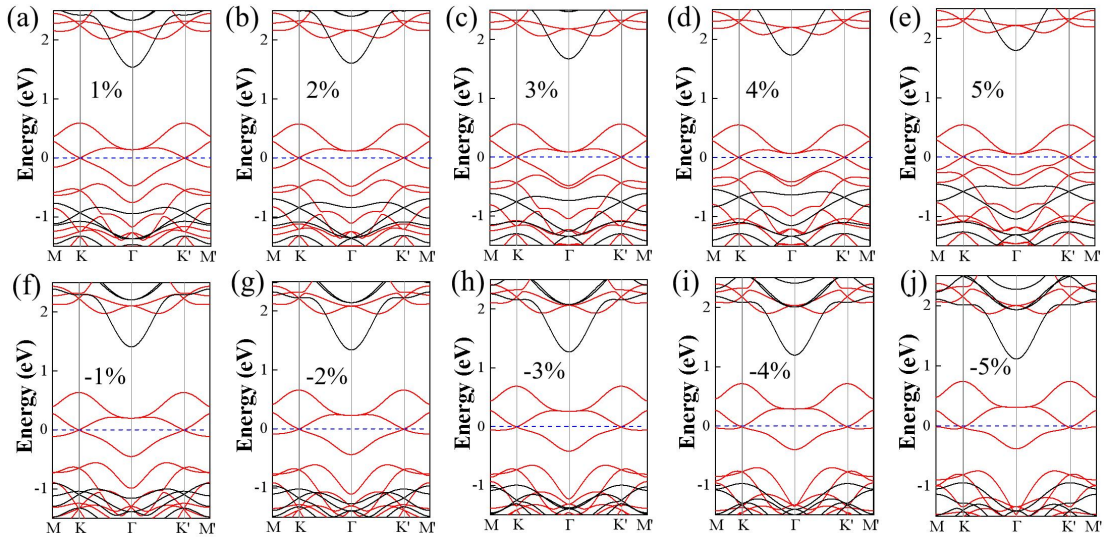

Figure S16. Band structures of $Cr_3S_2Se_2$ monolayer without considering SOC effect under biaxial strains from -5% to 5%.

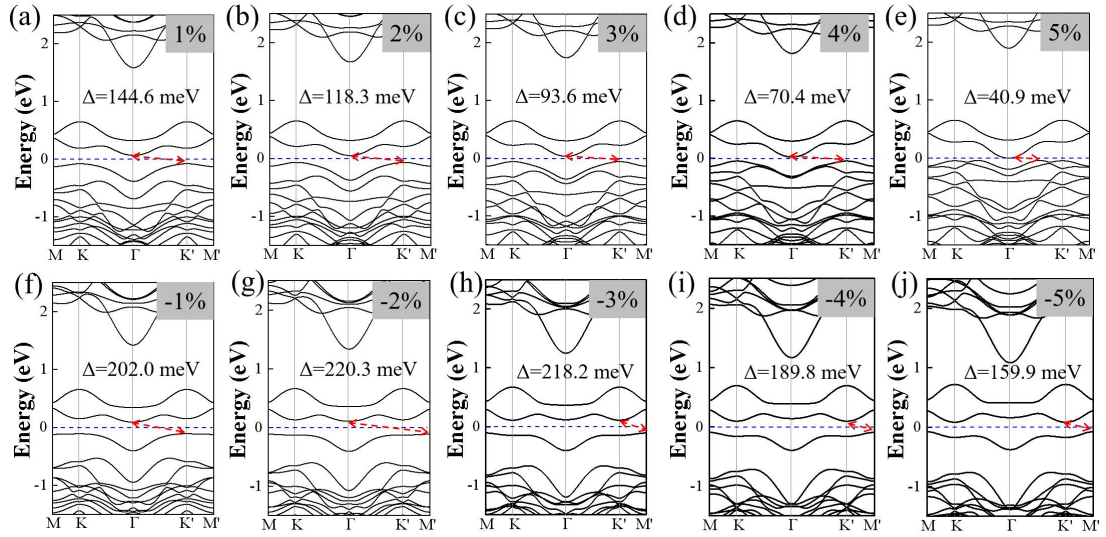

Figure S17. Band structures of $Cr_3S_2Se_2$ monolayer with considering SOC effect under biaxial strains from -5% to 5%.

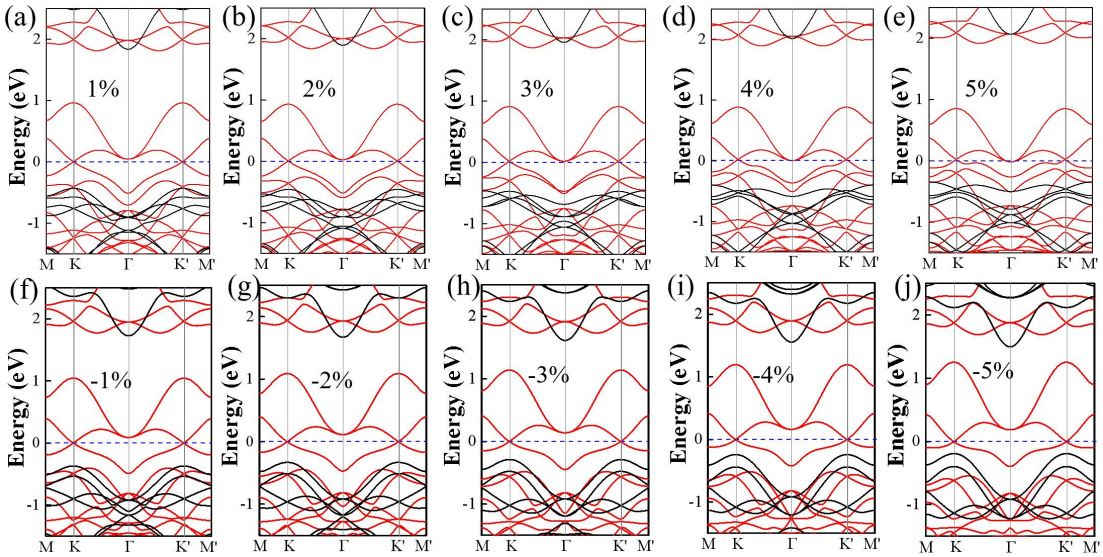

Figure S18. Band structures of $Cr_3Se_2Te_2$ monolayer without considering SOC effect under biaxial strains from -5% to 5%.

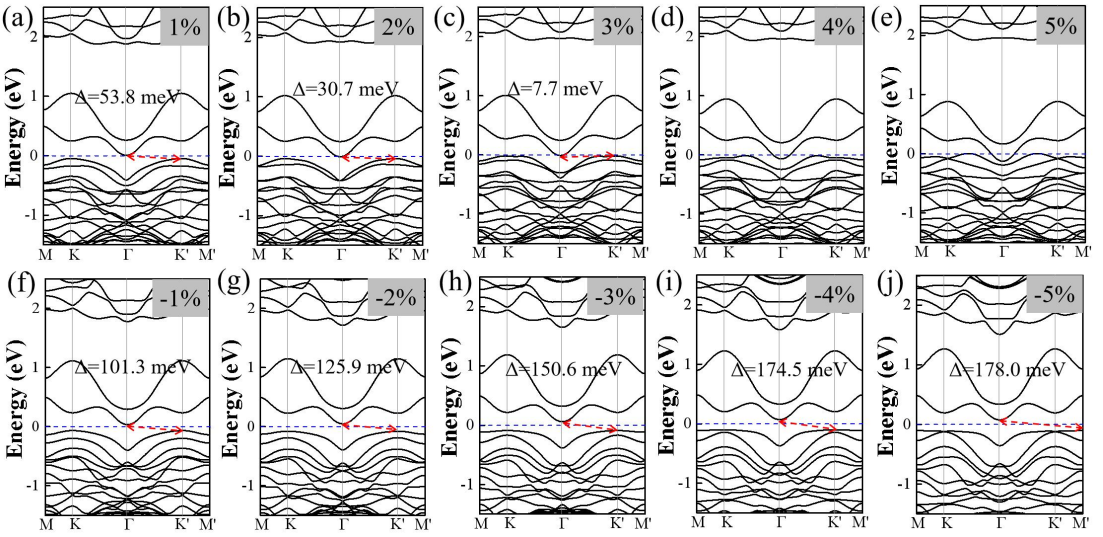

Figure S19. Band structures of $Cr_3Se_2Te_2$ monolayer with considering SOC effect under biaxial strains from -5% to 5%.

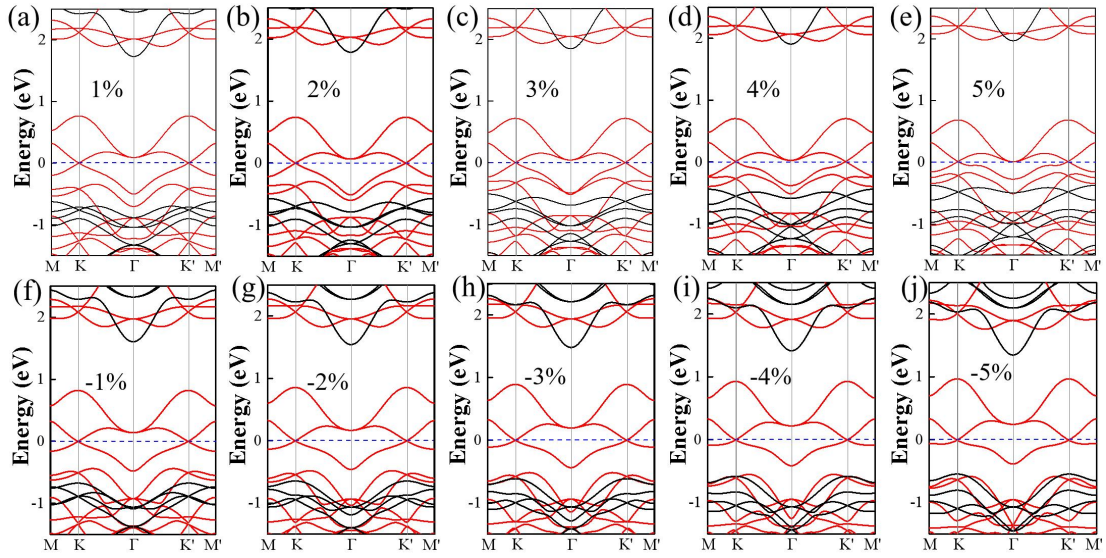

Figure S20. Band structures of $Cr_3S_2Te_2$ monolayer without considering SOC effect under biaxial strains from -5% to 5%.

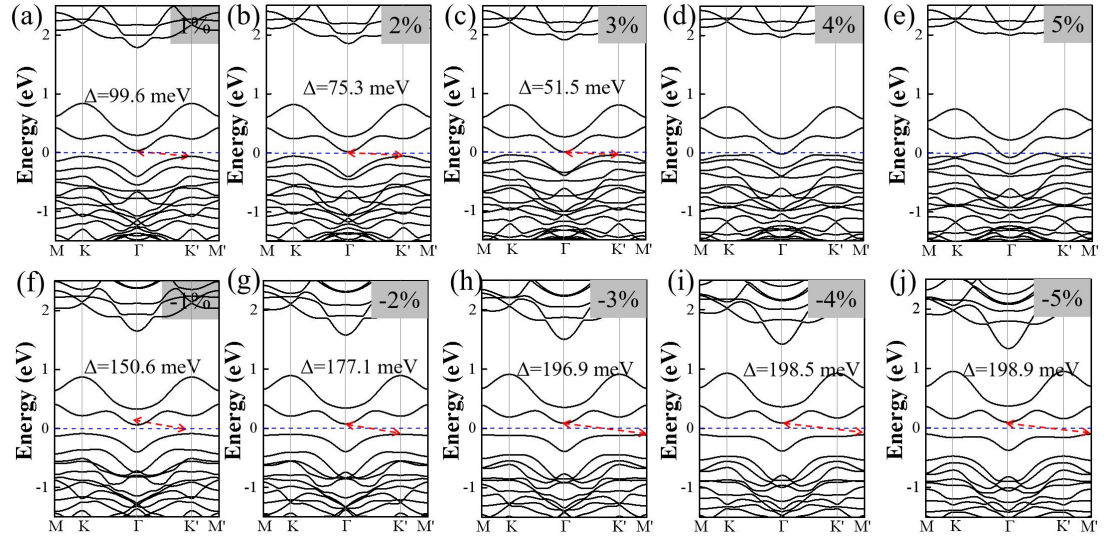

Figure S21. Band structures of $Cr_3S_2Te_2$ monolayer with considering SOC effect under biaxial strains from -5% to 5%.

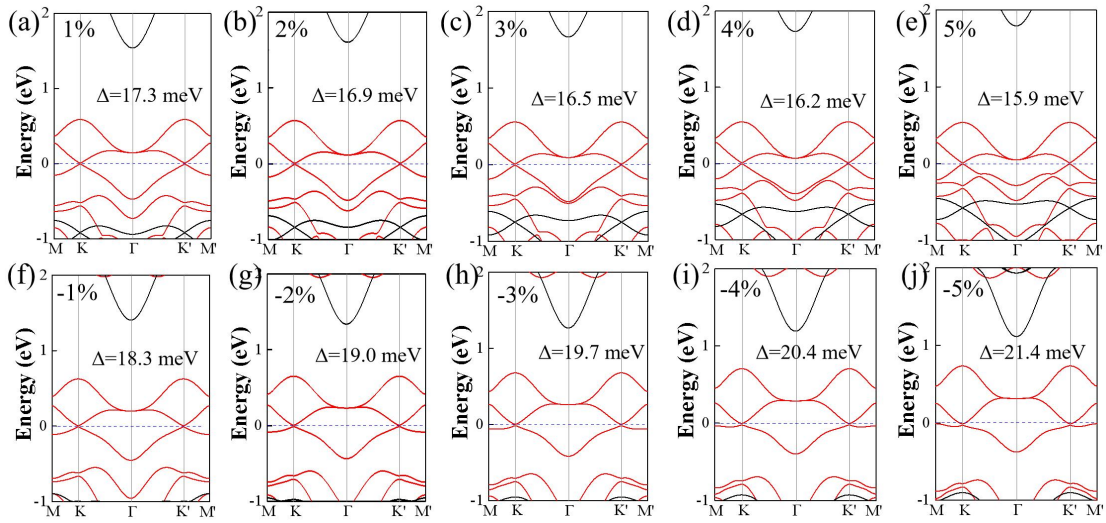

Figure S22. Band structures of $Cr_3S_2Se_2$ monolayer without considering SOC effect under electric field of 0.1 eV/Å and biaxial strains from -5% to 5%.

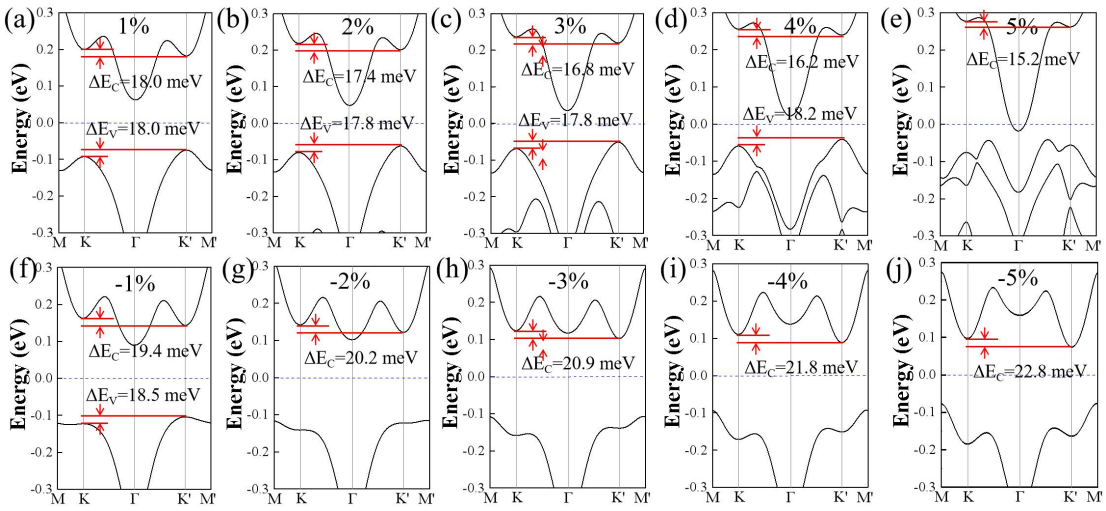

Figure S23. Band structures of $Cr_3S_2Se_2$ monolayer with considering SOC effect under electric field of 0.1 eV/Å and biaxial strains from -5% to 5%.

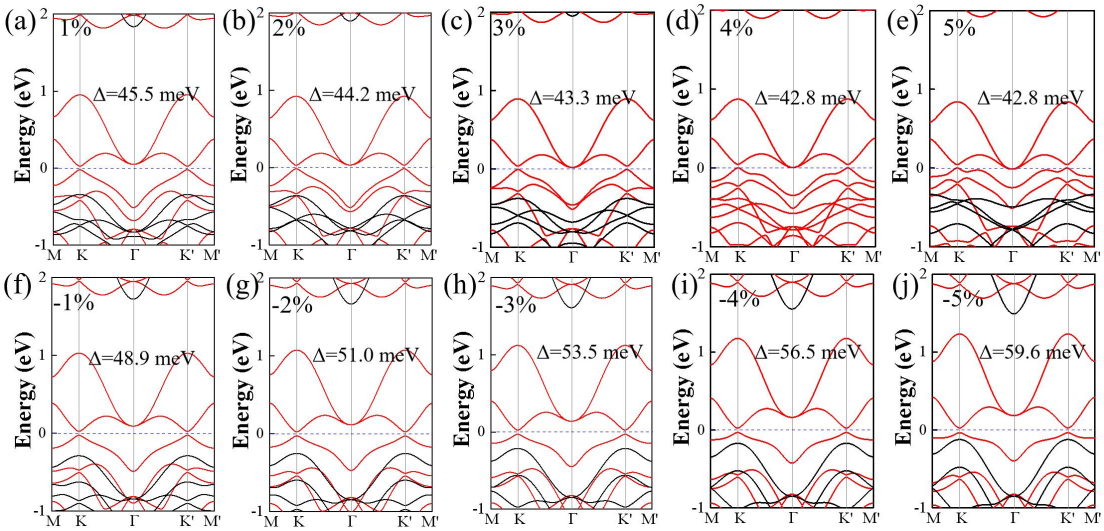

Figure S24. Band structures of $Cr_3Se_2Te_2$ monolayer without considering SOC effect under electric field of 0.1 eV/Å and biaxial strains from -5% to 5%.

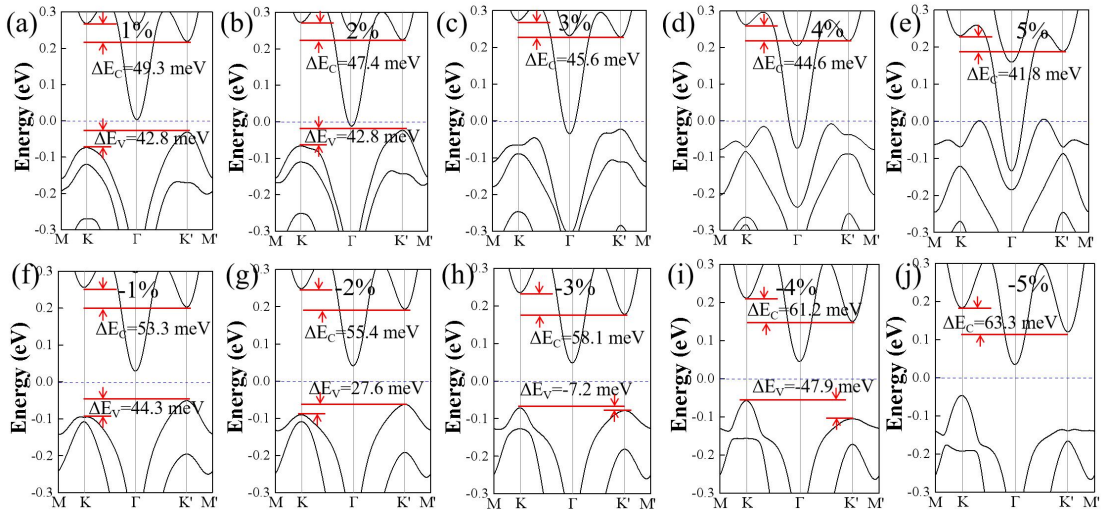

Figure S25. Band structures of $Cr_3Se_2Te_2$ monolayer with considering SOC effect under electric field of 0.1 eV/Å and biaxial strains from -5% to 5%.

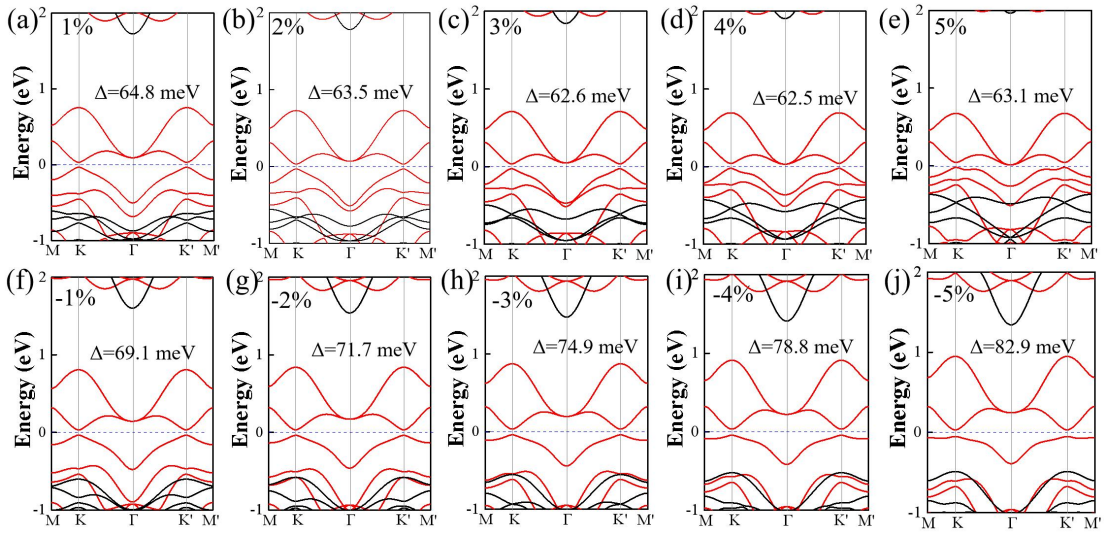

Figure S26. Band structures of $Cr_3S_2Te_2$ monolayer without considering SOC effect under electric field of 0.1 eV/Å and biaxial strains from -5% to 5%.

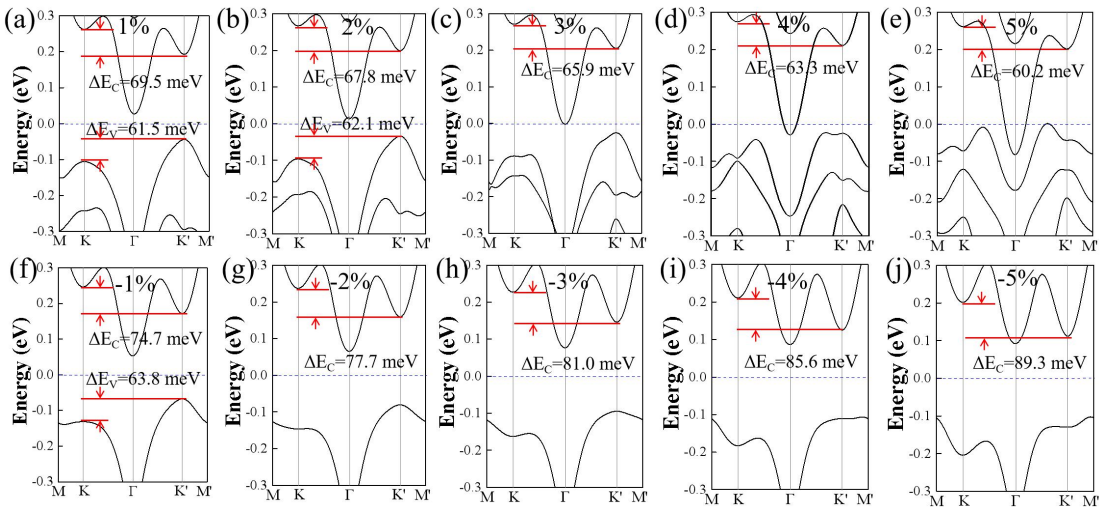

Figure S27. Band structures of $Cr_3S_2Te_2$ monolayer with considering SOC effect under electric field of 0.1 eV/Å and biaxial strains from -5% to 5%.

Part I: Calculation details for Curie temperature.

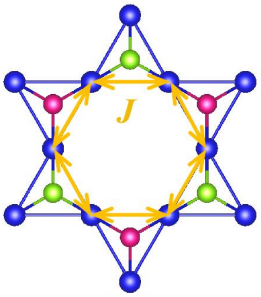

J is the nearest exchange parameter for $Cr_3X_2Y_2$ monolayer, blue, red and green balls

represent Cr, S and Se atoms, respectively.

The Hamiltonian based on 2D Heisenberg model is written as:

$$\hat{H} = -\sum_{i,j} J\vec{S}_i \cdot \vec{S}_j - \sum_i A(S_z^i)^2 \qquad \text{(S1)},$$

where J is the nearest exchange coupling parameter and the schematic is shown in Figure R1, S_i is the spin vector of Cr atom on site i. The J value can be extracted from

$$\begin{aligned} E_{FM} &= E_0 - 12J \times S^2 \\ E_{AFM1} &= E_0 - 4J \times S^2 \end{aligned} \qquad \text{(S2)}.$$

The exchange parameter J can be derived as:

$$J = (E_{AFM1} - E_{FM}) / 8S^2 \qquad \text{(S3)}.$$

The spin-spin correlation and critical temperature of $Cr_3X_2Y_2$ monolayer was evaluated by employing the EspinS package [*Comp. Mater. Sci.* 202, 110947 (2022)], in which 20×20 lattices were adopted in the MC simulations and the spins can randomly rotate in the space.